Inkjet Printed Single Walled Carbon Nanotube as an Interlayer for High Performance Thin Film Composite Nanofiltration Membrane

Myoung Jun Park [†1, a], Chen Wang[†1, a], Dong Han Seo[a], Ralph Rolly Gonzales[a, b], Hideto Matsuyama[b], Ho Kyong Shon[a]*

[a] *Centre for Technology in Water and Wastewater (CTWW), School of Civil and Environmental Engineering, University of Technology Sydney (UTS), New South Wales, Australia*

[b] *Center for Membrane and Film Technology, Kobe University, Kobe, Hyogo, Japan*

[†] These authors contributed equally in this work

[*]Corresponding authors: Ho Kyong Shon; Email: hokyong.shon-1@uts.edu.au; Tel.: +61 2 9514 2629; Fax: +61 2 9514 2633.

20   **Abstract**

21   Inkjet printing process enables rapid deposition of inks with precise amount and location.

22   Moreover, the process can be automated and provide control such as repetitive printing of the

23   inks. Utilizing the advantageous features of the inkjet printing process, we demonstrate the

24   synthesis of thin film composite (TFC) flat-sheet membrane for NF application where single

25   walled carbon nanotube (SWCNT) was deposited via an inkjet printing process, acting as an

26   interlayer between the polyamide (PA) selective layer and polyethersulfone (PES) MF

27   membrane support. By controlling the number of SWCNT printings on the PES membrane, we

28   investigated how the SWCNT interlayer thickness influences the formation of PA selective

29   layer. The best membrane performance was achieved from the TFC membrane synthesized

30   using 15 cycles of SWCNT printing, where both high water flux (18.24 ± 0.43 L m^{-2} h^{-1} bar^{-1})

31   and the high Na$_2$SO$_4$ salt rejection ($97.88 \pm 0.33\%$) rates were demonstrated. SWCNT

32   interlayer provided highly porous, interconnected structure with uniform pore size distribution

33   which led to the formation of a defect-free ultrathin PA selective layer. Designing of TFC

34   membrane using the SWCNT deposition via inkjet printing is the new approach and

35   successfully demonstrated the significant improvement in the NF membrane performances.

36   **Keywords:**

37   Nanofiltration, Inkjet printing, Interlayer, Single walled carbon nanotube, Thin film

38   composite

39

40

41

42

43

1. Introduction

Thin film composite (TFC) membranes are conventionally synthesized by interfacial polymerization (IP) which forms a thin active layer on top of a microfiltration (MF) or ultrafiltration (UF) membrane substrates, where two different monomers of m-phenylenediamine (MPD) or piperazine (PIP) and trimesoylchloride (TMC) are commonly utilized to synthesis a polyamide (PA) active layer [1-3]. Both water permeability and selectivity of the membranes are most crucially dependent on PA active layer properties, while porous membrane support provides a robust mechanical support for PA selective layer. To this date, nanofiltration (NF) membranes composed of a thin film PA layer on top of UF membrane have been successfully commercialized and currently being used in wide range of applications in desalination and wastewater treatments. However, there are still challenges remain when they are implemented in the real field, due to their trade-off dilemma between the intrinsic solvent permeability and solute selectivity [4].

An ideal NF membrane needs to exhibit both high water permeability and high removal rate of various dyes or multivalent salts and other contaminants [5]. It is well known that, the thickness of PA selective layer is inversely proportional to the solvent permeability. Therefore, a desired PA layer structure can be achieved by fabricating an ultra-thin selective layer which is less than 100 nm in thickness whereas conventional TFC PA membranes are composed of 200-300 nm thin PA active layer with 150-300 μm porous support layer. Importantly, properties of the PA layer could significantly be influenced by structure and the surface property of a porous support substrate [6-9]. Recently, various efforts have been made to improve the membrane performances (water flux and selectivity) and membrane stabilities. One of a notable strategy is by addition of an interlayer between the PA active layer and the microporous support substrate. For example, Livingston et al. successfully synthesized a ultrathin PA active layer with a thickness of 10 nm by utilizing a porous cadmium hydroxide

69   nanostrands as interlayer which covered the surface of polyimide ultrafiltration support

70   membranes and a follow up IP reaction [6]. The smooth and uniform nanoporous structure of

71   the nanostrands interlayer enabled the formation of a defect-free and ultrathin PA active layer,

72   which achieved outstanding improvement in solvent permeability while retaining its excellent

73   salt rejection capability. Inspired by this study, Zhu and co-workers used polydopamine (PDA)

74   coated single-walled carbon nanotube (SWCNT) as an interlayer which was deposited via a

75   simple vacuum filtration technique [10]. This hydrophilic and smooth PDA/SWCNT interlayer

76   induced the formation of defect-free, highly crosslinked PA selective layer with a thickness of

77   12 nm, which improved the NF membrane performances compared to the interlayer free TFC

78   membrane.

79   As noted in previous studies, deposition of interlayer using different nanomaterials played

80   an important role in improving the NF membrane performances [7-15]. However, those

81   conventional approaches such as vacuum filtration, dip-coating, spin-coating and layer-by-

82   layer (LBL) methods in deposition of materials, as an interlayer for TFC membrane

83   fabrications, often lead to poor controllability of the deposited material surface properties or

84   limited in scalability and in some cases producing unwanted wastes [7, 9, 10, 16, 17].

85   Meanwhile, inkjet printing process could be a promising candidate which can enable the

86   deposition of nanomaterial based interlayer uniformly. Inkjet printing is a versatile tool which

87   can deliver precise and rapid deposition of organic, polymeric materials and nanomaterials at

88   scale for various applications [18-22]. Moreover, conventional routes in depositing polymers

89   or nanomaterials often generated chemical and nanomaterial wastes which remains a

90   significant challenge. These material wastage issues can be minimized when depositing

91   materials via inkjet printing process as precise amount of material deposition is possible in this

92   process.

93 Therefore, such features of the inkjet printing process and inspired from the successful

94 implementation of inkjet printing process in other applications, this work aims to take the

95 advantage of the inkjet printing technology in membrane manufacturing, which will deliver

96 deposition of uniform nanomaterial interlayer with good controllability for high performing

97 TFC membrane synthesis. In general, inkjet printing process enable the deposition of picoliter

98 (2~30 pL/drop) scale of liquid drops through the number of nozzles from a print-head, with

99 frequencies of up to 2000 drops s^{-1} per nozzle [23]. Moreover, inkjet printing process provided

100 precise control in positioning of the polymer solution deposition at a high speed [24]. Due to

101 these advantages of inkjet printing technique, recent studies successfully demonstrated the

102 uniform coating of nanomaterials such as graphene, graphene oxide, metal organic frameworks

103 (MOF) and CNTs on a paper substrate for patterning of conductive materials [19, 25-27].

104 Furthermore, one study has successfully demonstrated the deposition of ultrathin and uniform

105 graphene oxide layer on a polymeric support membrane to synthesize a NF membrane for water

106 purification [28]. As such, use of inkjet printing in membrane manufacturing require further

107 exploration and demonstrations in diverse membrane synthesis applications to fulfill its

108 potential in bringing the efficient, precision controlled and scalable membrane manufacturing

109 into reality.

110 In this study, we demonstrate the deposition of uniform, smooth SWCNT layer via inkjet

111 printing process to serve as an interlayer between the PA active layer and PES MF membrane

112 which is first demonstration for NF application. Multiple number of SWCNT printings on the

113 PES membrane were conducted to investigate how SWCNT interlayers influenced the

114 formation of PA active layer using various membrane characterizations. Moreover, the

115 performance of fabricated TFC NF membranes were evaluated by water permeability and salt

116 rejection tests to find an optimal fabrication condition. The different surface characteristics of

117 SWCNT interlayers induced by different number of inkjet printing and the respective formation

of PA layer was further investigated. Our studies shed light on the control of PA selective layer in TFC membrane by introducing the uniform, nanomaterial based interlayer and demonstration the further use of inkjet printing process in membrane manufacturing which plays a crucial role in synthesis of high performing TFC membrane.

2. Experimental

2.1 Materials and chemicals

Hydrophilic PES microfiltration (MF) membrane filter with a pore size of 0.22 μm was used as membrane support (Sterlitech, USA). Carboxylated SWCNT (SWCNT, Purity: > 95 wt%, outer diameter (OD): 1-2 nm) powder with a short length (1~3 μm) was purchased from Jiangsu XFNANO Materials Tech CO., Ltd, China. Sodium dodecyl sulfate (SDS, ≥ 99.9%) from Sigma-Aldrich was used as the surfactant for SWCNT dispersion. For PA active layer formation, piperazine (PIP, 99% purity) and trimesoyl chloride (TMC, 98% purity) were purchased from Sigma-Aldrich and hexane (99.9% purity) from Merck was used as solvent for TMC. For evaluating the membrane performance, sodium chloride (NaCl), magnesium sulfate ($MgSO_4$), magnesium chloride ($MgCl_2$) and sodium sulfate (Na_2SO_4) were supplied by Chem-Supply Pty. Ltd., Australia. All chemicals in this study were used as received. A Milli-Q ultra-pure water system (Millipore) was used to produce deionized (DI) water and used in all experiments.

2.2 Inkjet printing of SWCNT ink on PES MF support membrane

The SWCNT ink was prepared by sonicating 200 mg of SWCNT powder in 200 mL of 1 mg mL^{-1} SDS water solution for 4 h using a probe type high power ultrasonicator under 80 W of power. Removal of impurities was conducted via a centrifugation of solution at 7,000 rpm for 30 min and followed by a supernatant dispersion was collected. This step was repeated 3~4

142 times until the stable solution is collected and the SWCNT solution with a final concentration

143 of ≈ 0.25 mg mL^{-1} was obtained and directly used as a SWCNT ink without adding further

144 additives.

145   A commercial Deskjet 2130 HP printer with a cartridge nozzle diameter of 30 µm was used

146 to print the SWCNT ink onto the surface of PES MF membrane support. The size and ejection

147 of an ink droplet is controlled by a HP thermal inkjet print technology. To prevent the

148 membrane surface damage, the front paper feed rollers and the rear roller at the middle of the

149 printer were removed prior to inkjet printing process as indicated in Fig. S1. A black ink from

150 a commercial black inkjet cartridge (HP 63 Genuie Black) was removed and carefully washed

151 and filled with prepared SWCNT ink in the presence of a sponge which prevents the leakage

152 of the ink through the nozzles (see Fig. 1A). Afterwards, the SWCNT ink cartridge was loaded

153 onto the printer. The PES MF membrane (size: 6 cm × 6 cm) was firmly bind to an A4-sized

154 polyethylene terephthalate (PET) film and was loaded into the printer. A computer was

155 connected to the printer and the printing software was set on maximum quality with 1200×1200

156 dpi. Then the SWCNT ink was subsequently printed on the surface of membrane substrate and

157 then dried in a controlled room temperature for 2 min. The number of printing was varied from

158 0, 5, 10, 15 and 20 repetitions to investigate the effect of SWCNT thickness coated on a

159 microporous PES membrane substrate as a function of interlayer. According to the number of

160 prints, SWCNT ink printed samples were denoted as P-0, P-5, P-10, P-15 and P-20 in this

161 paper.

162 *2.3 Fabrication of thin-film composite (TFC) membranes*

163   Fabrication of TFC membrane via and interfacial polymerization (IP) to form a PA layer on

164 the SWCNT-free (PES MF membrane) support and SWCNT-coated membrane supports was

165 conducted using two monomers of PIP and TMC (Fig. 1B), as similarly with our previous

166 studies [29, 30]. Prior to IP process, prepared membrane supports were first pre-wetted by

167 water without any alcohol treatment and stored in DI water for overnight. The remaining water

168 on the membrane surface was removed by a filter paper and then only one side of membrane

169 surface was allowed for exposure using an acrylic frame for introduction of PIP and TMC

170 monomers. Then a certain concentration of PIP aqueous solution (0.05− 0.2 wt%) was poured

171 on a membrane surface which was exposed to the air for 1 minute and followed by removal of

172 excess liquid by wiping them out using a filter paper. Subsequently, 0.1 w/v% of TMC in

173 hexane was then introduced onto the membrane surface for 30 s to allow the formation of a

174 thin film PA active layer via IP reaction. The membranes were then dried in air for 1 minute

175 and heat-cured to facilitate higher cross-linking of amine reaction in the oven at 65°C for 5

176 mins. The fabricated TFC membranes were then kept in DI water and stored in a refrigerator

177 at 4°C before use. The PA layers fabricated on the P-0, P-5, P-10, P-15, and P-20 membrane

178 samples were denoted as TP-0, TP-5, TP-10, TP-15 and TP-20, respectively.

179 *2.4 Characterization of membrane supports and TFC membranes*

180 The morphological investigations via a field emission scanning electron microscope (FE-

181 SEM) (Zeiss Supra 55VP, Carl Zeiss AG) operated at 5 kV were performed for both membrane

182 supports and TFC membranes. For observing cross-section SEM images of TFC membranes,

183 a piece of TFC membrane was soaked in liquid nitrogen to fracture the samples. All membranes

184 were sputtered with Pd/Au using a coating machine (EM ACE600, Leica) before the FE-SEM

185 characterization. Surface hydrophilic property of membrane supports was estimated by water

186 contact angle measurements using an optical tensiometer (Theta Lite 100, Republic of Korea)

187 equipped with an image processing software. All support membranes were washed with DI

188 water to remove any impurities and post treatment agents and then dried at room temperature

189 prior to analysis. At least five measurements for each samples were examined and obtained an

190 average value. Surface mean roughness (R_a, nm) of SWCNT-free and SWCNT-coated

191 membrane supports was measured by atomic force microscope (AFM, Park X7) images with a

192 scanning area of 5 µm × 5 µm and three measurements for each samples were performed and

193 their average values were obtained. Additionally, an overall average pore size of membrane

194 supports were determined using a capillary flow porometry (Porolux 100) under dry-up/wet-

195 up mode and a low surface tension Porefil (16 dynes cm^{-1}) was used as a membrane wetting

196 agent. To determine the atomic composition and degree of cross-linking of the PA layer in each

197 TFC membrane, X-ray photoelectron spectroscopy (XPS, JPS-9010 MC, JEOL, Japan)

198 analysis was performed. Based on the atomic composition analysis, the ratio of O and N can

199 provide the degree of cross-linkage of the PA layer. The O/N ratio is inversely proportional to

200 the degree of cross-linkage, which can be calculated using Eqns. (1) and (2):

201 $$a + b = 1 \tag{1}$$

202 $$\frac{O}{N} = \frac{3a+4b}{2a+2b} \tag{2}$$

203 where a and b are the fractions of the crosslinked structure and linear structure components of

204 PA layer, respectively.

205 The surface zeta potential of TFC membranes was evaluated using an Anton Paar Surpass

206 solid-surface analysis. All zeta potential tests at different pH (3-10) were carried out with 1

207 mM KCl background solution at 25°C and the solution pH values were adjusted by dosing 0.1

208 M HCl or 0.1 M NaOH solution.

2.5 Evaluation of separation performance for TFC membranes

210 TFC membrane performance such as water permeation and salts rejection was evaluated

211 using a Lab-scale membrane testing machine under cross-flow operation mode (cross-flow

212   velocity = 8.3 cm s^{-1}) with effective membrane area of 4 cm^2. Permeate water flux and salt

213   rejection rates were determined under the testing pressure of 4 bar at a temperature of 23°C ±

214   1. Prior to performance tests, membrane samples were pre-compacted with DI water for 30 min

215   to minimize the effect of membrane compaction on membrane performance. The permeate flux

216   J_w was calculated using Eq. (3):

217     $$J_w = \frac{V}{A\Delta t}$$ (3)

218   where V is the volume of the permeate water (L), A is the effective membrane area (m^2), and

219   Δt is the time interval (h).

220   For the evaluation of the salt rejection performance, each 1,000 mg L^{-1} of Na$_2$SO$_4$, MgSO$_4$,

221   MgCl$_2$ and NaCl salts were used as feed solutions and the conductivity of the feed and permeate

222   solutions were measure using a portable conductivity meter (D-74G, Horiba scientific, Kyoto,

223   Japan) to evaluate the salt rejection performance of the TFC membranes.

224   Salt rejection R was calculated by Eq. (4):

225     $$R \ (\%) = 100 \ \times (1 - \frac{C_p}{C_f})$$

226   (4)

227   where C_f and C_p are the salt concentrations in feed and permeate, respectively.

228

229   **3. Results and discussion**

230   ***3.1 Effect of SWCNT deposition via inkjet printing on PES MF membrane supports***

231   The SWCNT interlayer deposition on the PES MF support membrane was conducted via

232   inkjet printing technology. The prepared SWCNT ink was smoothly printed on the membrane

233   substrate and did not observe any blockage of nozzles in the cartridge head during the whole

234   printing experiments (See supplementary video S1). The effects of coated SWCNT layer on

235   the properties and morphology changes of PES membrane surface were investigated as these

236   two parameters strongly influence the formation of PA layer during the IP process. Fig. 2 shows

237   the FE-SEM and AFM images of support membranes without SWCNT interlayer and with

238   SWCNT interlayer coating. Pristine PES (P-0) MF membrane surface reveals a plane

239   polymeric surface with micron-sized open pores. However, as the numbers of SWCNT ink

240   printed on the membrane support increased, the open pores on the membrane surface were

241   covered by SWCNT network. When the 15 printings of SWCNT ink were performed, open

242   pores on the PES membrane surface were fully-covered with SWCNT network. For instance,

243   micro-pores on the PES membrane surface for P-15 and P-20 samples, disappeared over the 15

244   cycle of SWCNT ink prints, where SEM images exhibit continuous and dense-compact

245   SWCNT network formation on the surface of the PES membrane support. The volume of each

246   ink drop of the ink cartridge 63 is around 22×10^{-12} L, and each drop covers an average surface

247   area of $90\times1,000$ μm^2 [28]. Therefore, 1 mL of SWCNT ink can covers about 410 cm^2 area of

248   membrane surface and for SWCNT ink with the concentration of ≈ 0.25 mg ml^{-1} can deposit

249   0.00061 mg cm^{-1}. In case the printing of 15 and 20 cycles can deposit SWCNT of 0.0092 and

250   0.0122 mg cm^{-2}, respectively, as indicated in Table 1. This calculation indicates that only small

251   amount of SWCNT (0.01 mg) was needed to effectively form a SWCNT network with full

252   coverage on the 1 cm^2 area of PES membrane support demonstrating the material efficiency of

253   the inkjet printing process. An accumulation of SWCNT in different printing numbers can also

254   apparently be distinguishable from the optical images exhibited in Fig. S2. The PES membrane

255   surface has revealed darker grey colors with increase in SWCNT printing numbers.

256
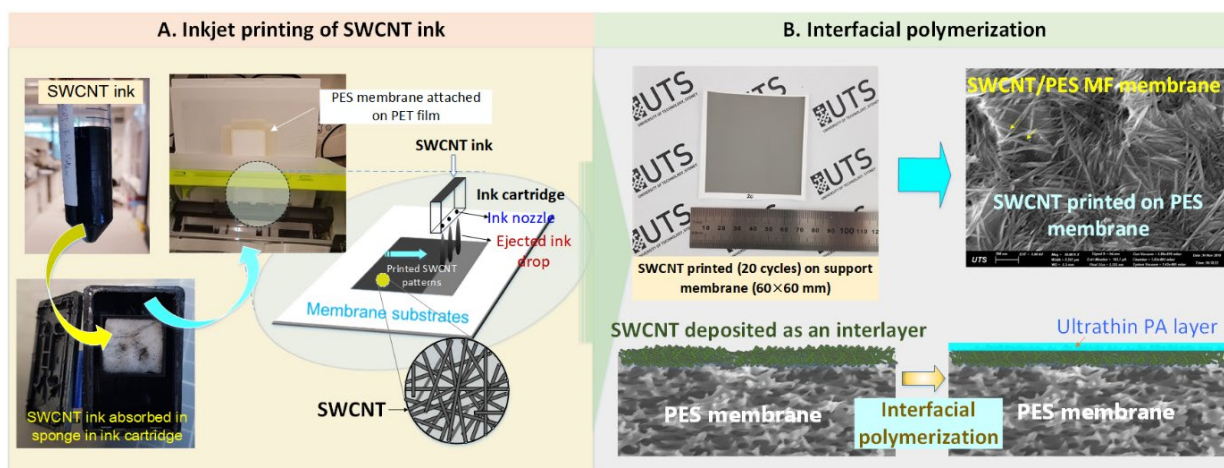
Fig. 1. Schematic of (A) SWCNT deposition on PES MF membrane via inkjet printing and

(B) ultrathin PA active layer deposition onto SWCNT coated PES membrane via interfacial

polymerization (IP).

Table 1. Pure water permeability, contact angle, average pore size and deposited SWCNT
amount of SWCNT-coated samples respect to the number of SWCNT ink prints.

| Sample	Number of SWCNT ink prints	SWCNT amount (mg cm^{-2})	Average pore size (nm)	Pure water permeability (L m^2 h^1 bar^{-1})	Contact angle [a] (Deg)
P-0	0	0	274.0	4505 ± 509	68.12 ± 2.20
P-5	5	0.0031	219.9	4057 ± 816	69.50 ± 3.13
P-10	10	0.0061	128.2	3427 ± 222	59.87 ± 2.69
P-15	15	0.0092	93.2	2332 ± 180	78.49 ± 4.16
P-20	20	0.0122	53.5	495 ± 42	83.19 ± 1.61

262 [a] Contact angle of water droplet measured at 0 sec.

263
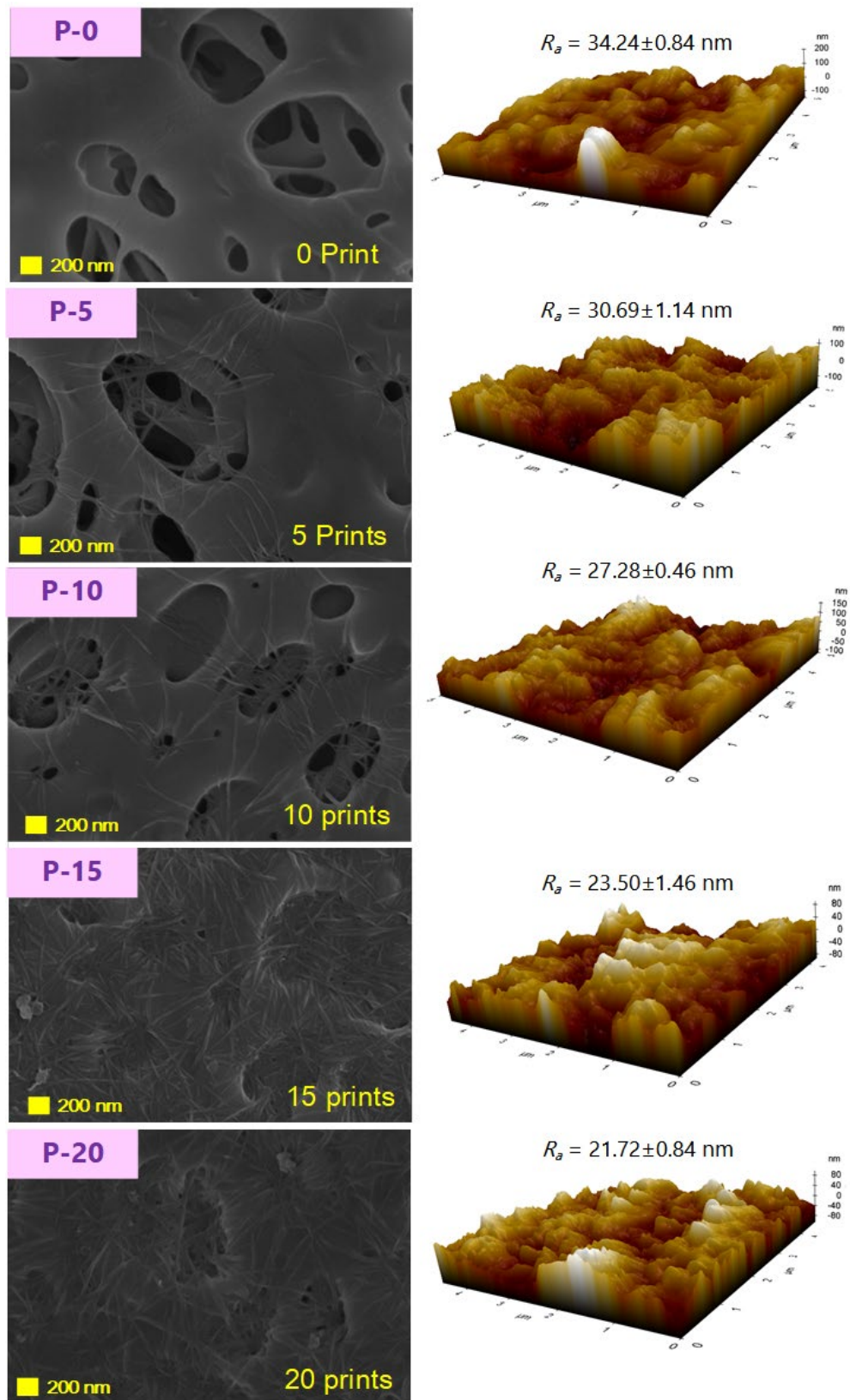
Fig. 2. FE-SEM and AFM images of the surfaces profile of PES MF membranes and the

SWCNT interlayer deposited PES membranes (P-0, P-5, P-10, P-15 and P-20).

266 From AFM images (right hand side figures from the Fig. 2), one can observe that with

267 increasing number of SWCNT printing, the surface roughness (R_a) value gradually decreased.

268 The P-0 showed an average surface roughness value of 34.24 ± 0.84 nm and then it decreased

269 to 30.69 ± 1.14 nm, 27.28 ± 0.46 nm, 23.50 ± 1.46 nm and 21.72 ± 0.84 nm for P-5, P-10, P-

270 15 and P-20, respectively. These results demonstrate that SWCNT layer provides a smoother

271 and denser surface with increasing number of SWCNT deposition. Meanwhile, the initial water

272 contact angle of the membranes (Table 1) slightly decreased as the number of SWCNT ink

273 printings increased up to 10 cycles. Without SWCNT interlayer deposition, the initial water

274 contact angle was 68.12°; however, it was decreased to 59.87° after 10 cycles of SWCNT

275 printing. The reduction of contact angle is mainly attributed to the presence of hydrophilic

276 carboxylated SWCNT coating on the PES support, and the clear trend can be seen from the

277 time profile measurement shown in Fig. 3. The P-5 (69.50°) membrane had the similar initial

278 contact angle with the P-0. However, there is a sharper drop of the contact angle appeared for

279 P-5 sample with time and the water droplet completely disappeared after 9 s, and more

280 significant reduction was observed for P-10 sample. In contrast, it can be noted that when the

281 number of SWCNT prints exceeded 15 cycles (P-15 and P-20 samples), the contact angles were

282 increased compared to that of P-0 sample. This is due to the more densely packed SWCNT

283 network structure with increased deposition amount of the SWCNT leading to significant

284 decrease in pore size of the membrane (see Table 1). Thus, reduced pore size might hindered

285 the rapid penetration of water droplet, resulting in slight increase of the water contact angle

286 and similar trends are also observed from previous literatures [12, 31]. The pure water flux of

287 the support membranes (before IP process) was also measured to see the impact of SWCNT

288 deposition on the membrane performance. As shown in Table 1, the SWCNT-free PES support

289 (P-0) revealed the pure water flux of 4545.1 L m^{-2} h^{-1} bar^{-1} which is typical permeability value

290 for MF membranes and then there was a gradual flux decline observed from 4057.5 to 2332.5

291   L m^{-2} h^{-1} bar^{-1} with increasing number of SWCNT printings from 5 to 15 printing cycles,

292   respectively. Further to this, it can be noted that there was a considerable drop in water flux for

293   P-20, where 10 fold reduction in flux was observed (495.0 L m^{-2} h^{-1} bar^{-1}) compared to the P-

294   0 membrane. This result is due to the significant decrease in membrane pore size by

295   accumulation of SWCNT layer induced by repeated cycles of printing and these results are in

296   good agreement with the contact angle measurement. Average pore size of support membranes

297   was also measured for further confirmation and it is summarized in Table 1, and this result

298   supports the pure water flux measurement results. As noted in Table 1, the average pore size

299   was reduced when the printing number of SWCNT was increased. The average pore size of

300   274.0 nm was obtained for pristine PES support membrane (P-0) and this value is well-matched

301   with the manufacturer's information (220 nm). Eventually the pore size reached to 53.5 nm by

302   20 cycles of SWCNT ink printing which represented similar pore size of typical UF membranes.

303   These results support that SWCNT layer coated on the PES MF membrane, significantly

304   changed the surface morphology, and induced by varying deposition amount of SWCNT which

305   was controlled by the number of printing cycles. Such parameter altered the compactness of

306   the SWCNT network on PES support, thus reducing the pure water flux, surface pore size and

307   the surface roughness, while increasing the contact angle of the membrane support. All these

308   results are also consistent comparing with the previous studies which used CNTs as an

309   interlayer for high performance NF membrane fabrication [8, 10-12, 31, 32].

310
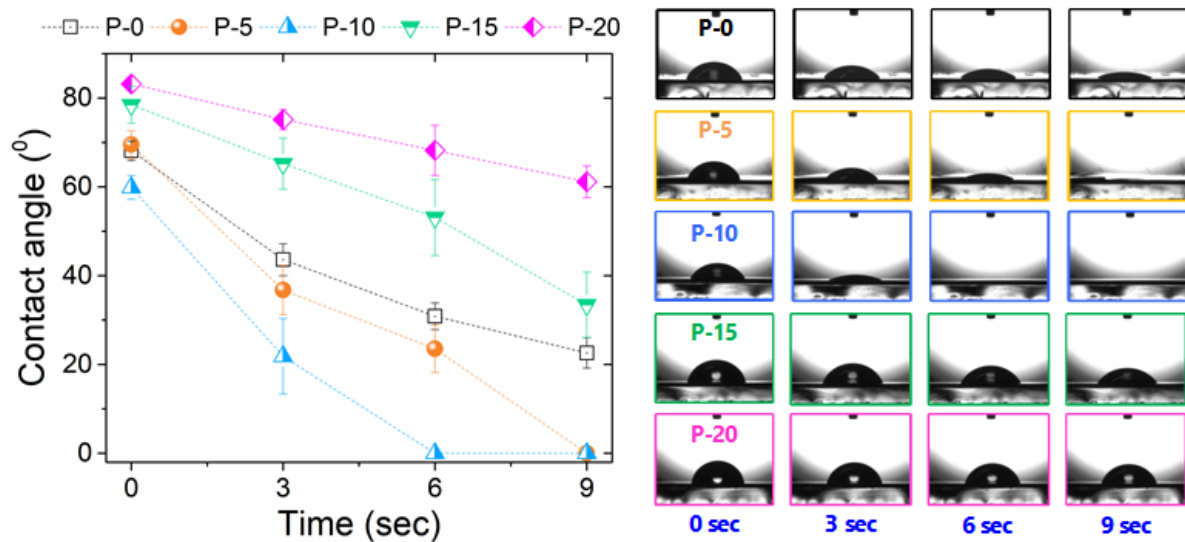
Fig. 3. Contact angle trend of membrane supports as a function of contact time.

312

3.2 Optimization of IP condition at different PIP concentrations

314 Effect of PIP concentrations on NF membrane performance was investigated to find out an

315 optimum IP condition as well as a role of SWCNT interlayer. Two samples of pristine PES MF

316 membrane support (P-0) and SWCNT deposited on PES support by 10 SWCNT ink printings

317 (P-10) were used to conduct the IP process to compare the NF performance and their

318 corresponding TFC membranes were denoted to TP-0 and TP-10, respectively. The PIP

319 monomer concentration was varied at 0.05, 0.1, 0.15 and 0.2 wt% while the TMC concentration

320 was fixed at 0.1 w/v% for the formation of PA layer on the membrane substrates. Fig. 4

321 represents the permeate water flux and salt rejection (Na_2SO_4 1,000 mg L^{-1} as feed solution)

322 performances of TP-0 and TP-10 TFC-NF membrane samples tested under applied pressure of

323 4 bar. Overall, both TP-0 and TP-10 TFC membranes exhibited similar water flux and salt

324 rejection trend as a function of different PIP concentrations in IP process, where the water flux

325 decreased while Na_2SO_4 divalent salt rejection improved as PIP concentration was increased.

326 This is mainly attributed to the less defects are formed in the PA selective layers when PIP

16

327   monomer concentration is increased, which resulted in increasing water transport resistance

328   indicating the reduction of water flux but improving the salt retention across the thin PA

329   selective layer. Such observation is also supported by previous literatures [10, 14]. From the

330   performance trend shown in Fig. 4, TP-10 membrane was less affected by the PIP

331   concentrations compared to TP-0 membrane in membrane performances. Water flux of 19.98

332   L m^{-2} h^{-1} bar^{-1} was observed for TP-10 membrane showing slightly higher value compared to

333   the TP-0 membrane (18.65 L m^{-2} h^{-1} bar^{-1}) at low PIP concentration of 0.05 wt%. However,

334   there is considerable decline in water flux for TP-0 membrane observed with increase in PIP

335   concentration, where water flux declined by 50% to 9.35 L m^{-2} h^{-1} bar^{-1} at the PIP concentration

336   of 0.2 wt%, while only 24% (16.88 L m^{-2} h^{-1} bar^{-1}) was reduced for TP-10 membrane under the

337   same PIP concentration.
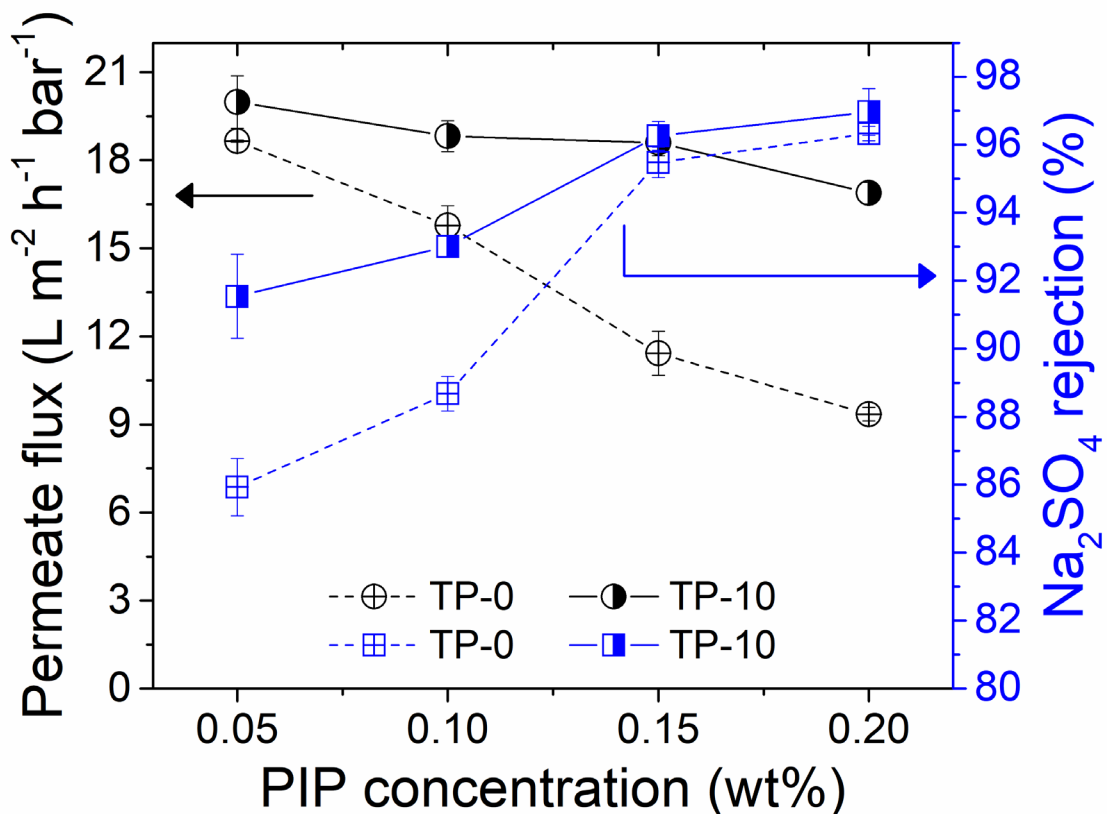
338

339   **Fig. 4**. Permeate flux and salt rejection (Na_2SO_4 1,000 mg L^{-1}) performance of NF

340   membranes for TP-0 and TP-10 TFC membranes fabricated under different PIP

341   concentrations (0.05, 0.1, 0.15 and 0.2 wt%).

342   Meanwhile, a significant improvement in Na_2SO_4 rejection was observed for TP-10 membrane

343 with increase in PIP concentration. The result shows that salt rejection rate was increased from

344 91.54% to 96.26% at PIP concentration ranging from 0.05 wt% to 0.15 wt%, respectively, and

345 this result is comparable to the level of typical NF membranes performance. Although the TP-

346 0 membrane also followed a similar trend, by showing improvements in salt rejection rate, yet

347 its Na_2SO_4 rejection rate was lower values than that of P-10 membrane at all PIP concentrations.

348 From the above experimental results, it can be deduced that the membrane support surface

349 modified with SWCNT interlayer with 10 cycle of prints, provided the surface condition for

350 stable and enhanced polymerization to occur by reducing average pore sizes from 274 nm (P-

351 0) to 128.2 nm (P-10) with porous and interconnected matrix, which helped the formation of

352 defect-free and thin PA active layer even at relatively low PIP concentrations. Therefore, the

353 optimum IP condition for this study was selected at the PIP concentration of 0.15 wt% which

354 exhibited minimal decline in water flux while maintaining a good salt rejection rate (> 95%).

355 *3.3 Effect of SWCNT as an interlayer on the PA active layer formation*

356   Formation of PA selective layer on the surface of membrane supports were performed via IP

357 process using PIP (0.15 wt%) and TMC (0.1 wt%) monomers, and the surface morphologies

358 and the thickness of PA layers were characterized by FE-SEM. Fig. 5 illustrates the top surface

359 (left) and cross-sectional (right) images of PA layer for TFC-NF membranes without SWCNT

360 deposition (TP-0) and with SWCNT deposition (TP-5−20) representing the different numbers

361 of inkjet printing cycles. Considerably rough and nodular shapes of PA was formed on the top

362 surface of the SWCNT-free membrane (TP-0) which is shown in Fig. 5 and one can expect that

363　there would be some defects formed during the PA formation. Moreover, one can notice that

364　the PA layer was formed inside the large pores of PES MF support (pore size of 274 nm) as

365　indicated by red arrows on the top surface SEM image of TP-0. This might be formed from the

366　remaining PIP monomer entrapped within the micropores, due to the large, rough, and

367　discontinuous pore structure of the PES substrate. This resulted in the non-uniform distribution

368　of PIP on the substrate, and subsequent formation of discontinuous, thick, and relatively rough

369　PA surface layer [31, 32]. On the other hand, smoother and flatter PA layer is formed when the

370　number of SWCNT interlayer depositions was increased as shown in Fig. 5. Patterns of

371　micropore of the membrane surface became less obvious or disappeared in the orders of TP-5,

372　TP-10, TP-15 and TP-20 membranes when covered with PA layer. It clearly indicates that

373　uniformly-dispersed and deposited SWCNT interlayer led to the reduced pore size with smooth

374　membrane surface, which helped the uniform diffusion of PIP solution, thus resulting in a

375　formation of defect-free, continuous, and smooth PA active layer. More details on PA layer

376　formation without and with SWCNT interlayers on PES membrane support will be discussed

377　in Section 3.5.

378　Furthermore, the thickness of PA active layer was significantly reduced as SWCNT ink

379　printing numbers increased, as revealed in the cross-sectional images in Fig. 5 (right hand side).

380　The TP-0 sample (SWCNT free) exhibited PA layer thickness of 123.5 ± 9.4 nm. However,

381　when the SWCNT ink was printed more than 10 cycles, the thickness of PA active layer was

382　observed to be less than < 60 nm. Ultrathin PA active layer was consistently formed with

383　thickness of ~42 nm when the SWCNT ink printing exceeded 15 cycles as can be clearly seen

384　in Fig. 5 and Fig. S3. SWCNT layer provided the reduced pore size and interconnected pore

385　matrix with increased surface porosity which would facilitate the formation of ultrathin PA

386　layer [32].

387
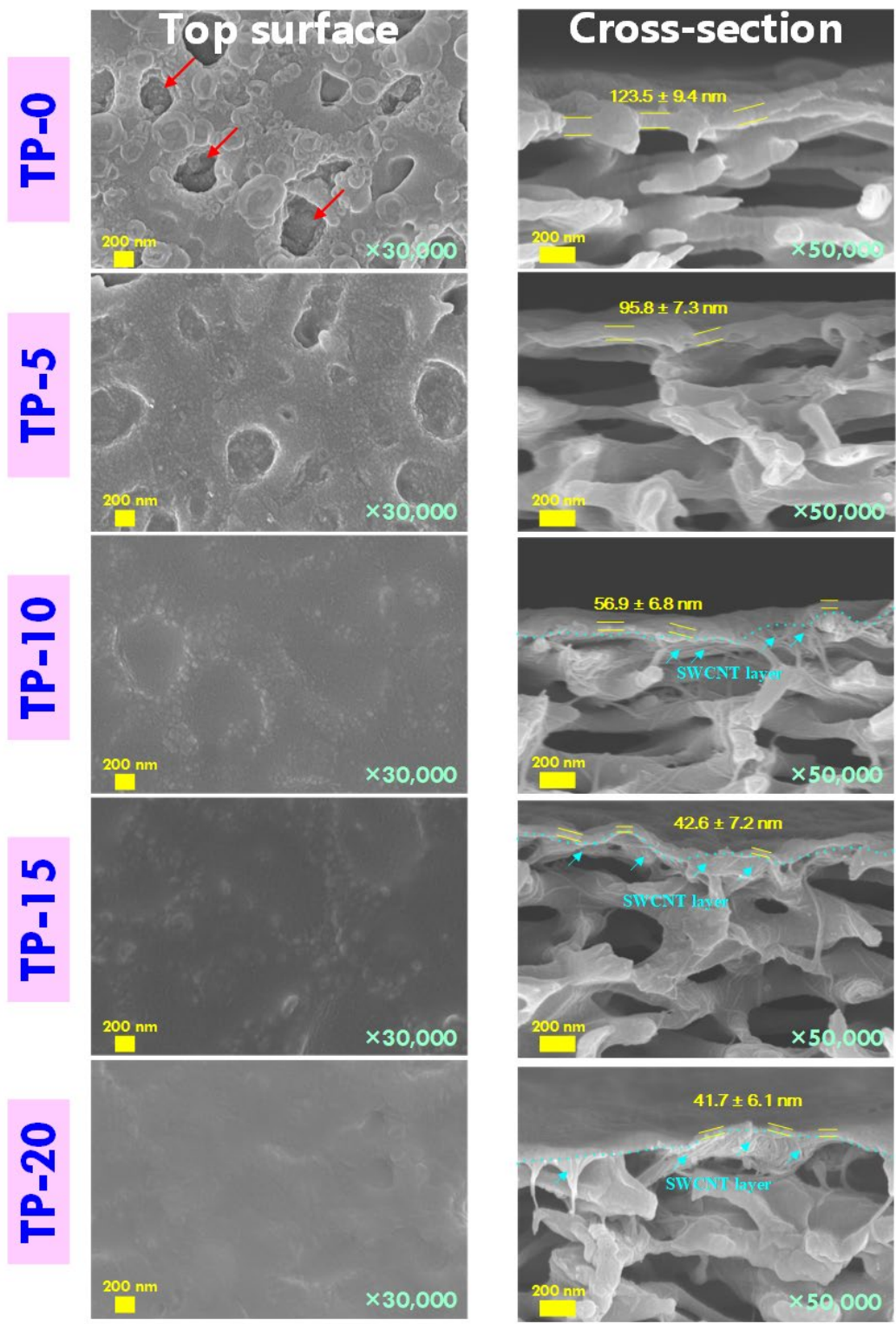
Fig. 5. Surface and cross-sectional FE-SEM images of the TFC NF membranes with different number of SWCNT ink printings.

388

389
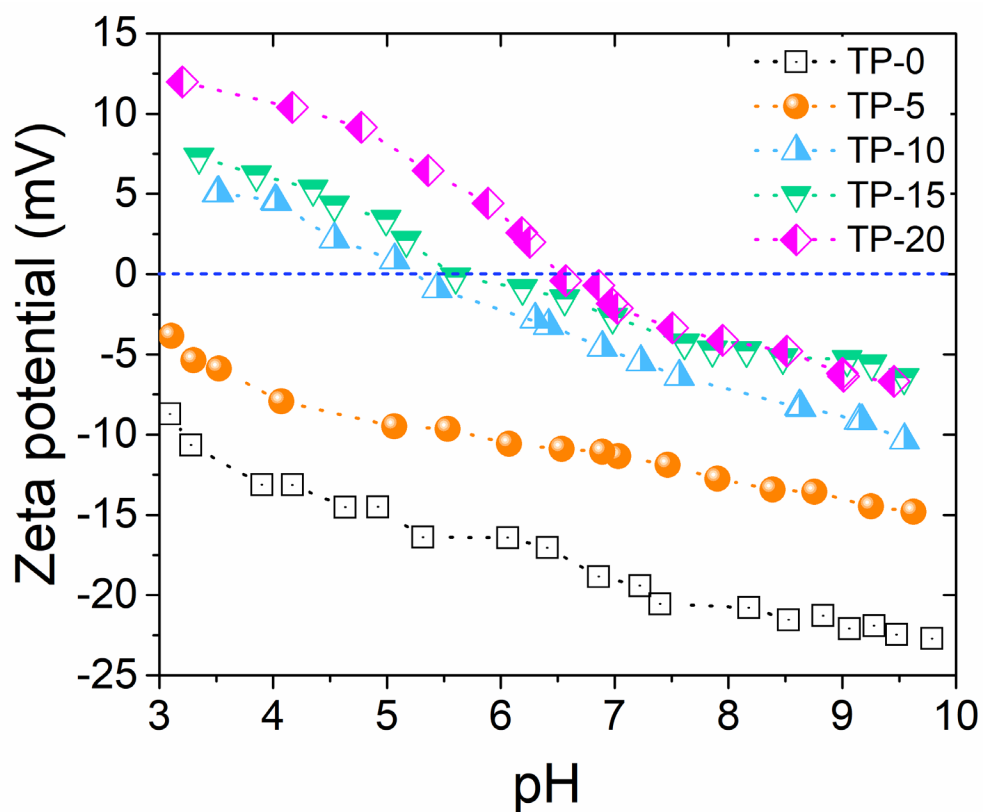
Fig. 6. Surface zeta potential of TFC membranes estimated at different pH (3-10).

Table 2. Atomic composition and the degree of cross-linking of PA layer in the TFC membranes.

Samples	C1s	O1s	N1s	O/N Ratio	Degree of cross-linking (%)
TP-0	74.83	15.44	9.73	1.59	32.04
TP-5	72.45	16.80	10.75	1.56	34.23
TP-10	76.15	14.47	9.38	1.54	36.09
TP-15	75.44	13.79	10.77	1.28	63.18
TP-20	74.66	14.07	11.27	1.25	66.91

As surface charge of the PA layer plays an important role in rejection of divalent anions due to the Donnan effects, surface zeta potential of TFC membranes at varying pH ranges (3-10) were

21

398   measured as shown in Fig. 6 [17]. The TP-0 membrane showed negatively charged surface

399   across the entire pH range from 3 to 10 and the zeta potential value gradually decreased with

400   increase of pH value. All TFC membranes revealed negative charges at an isoelectric point due

401   to the presence of uncross-linked carboxyl groups of the acyl chloride from the IP process [12].

402   It can be noted that the zeta potential values for PA layers were shifted from negative to positive

403   with increased number of SWCNT prints. In case of TP-15 membrane, the isoelectric point

404   (IEP) revealed at pH value of ~5.6 which is significantly increased as compared to the TP-0

405   membrane, yet it still exhibit negative charges which is in good agreement with other literatures

406   that PA layer formed on the SWCNTs intermediate layers, favorable IEP value for high

407   rejection of anions [12, 31]. Additionally, overall zeta potential trend with different amount of

408   SWCNT prints for the interlayer also well-matched with the degree of cross-linking (%) of PA

409   layer determined from the XPS analysis (Table 2). The lowest degree of cross-linkage was

410   obtained from TP-0 membrane (32.04%) which may correspond to the remaining of abundant

411   uncross-linked carboxyl groups on the PA surface as zeta potential result also demonstrate

412   significantly lower values across the pH ranges. However, as the SWCNT printing increased

413   from 5 to 20 cycles on the PES support for TFC membranes, lower negative charge were

414   exhibited and higher degrees of cross-linkage of PA layers were achieved at 34.23%, 36.09%,

415   63.18%, and 66.91% for TP-5, TP-10, TP-15 and TP-20, respectively. Such formation of highly

416   cross-linked PA layer was facilitated by SWCNT interlayer and could potentially be

417   advantageous for high ion selectivity driven by size sieving effect.

418   *3.4 Impact of SWCNT interlayer on TFC membrane performance*

419   In order to investigate the impact of varying number of SWCNT printings and interlayer

420   condition on TFC membrane performances, a PA layer was fabricated under optimum IP

421   condition of (PIP concentration of 0.15 wt% and TMC concentration of 0.1 w/v%) which was

422   obtained from the experimental results indicated in Fig. 4. The NF performance tests were

423   performed using a divalent salt of Na_2SO_4 for testing TFC membranes and water flux and salt

424   rejection performance results are represented in Fig. 7(A). It can be clearly seen that water flux

425   and Na_2SO_4 rejection of 11.42 ± 0.74 L m^{-2} h^{-1} bar^{-1} and $95.48 \pm 0.45\%$ is achieved for TP-0

426   sample and much enhanced performance where water flux of 18.60 ± 0.44 L m^{-1} h^{-1} bar^{-1} and

427   rejection of $96.26 \pm 0.42\%$ is achieved for TP-10 membrane. The trend shows that the

428   membrane performance steadily improved with increasing numbers of SWCNT prints from 0

429   to 10 cycles. After 10 cycles of SWCNT printing, marginal reduction in water flux appeared at

430   15 cycles of printings yet the salt rejection rate was further enhanced up to $97.88 \pm 0.33\%$.

431   Particularly, significant enhancement in permeate water flux (increment in water flux of 61%

432   from TP-0 to TP-10 membrane) was observed for TP-0 to TP-10 membrane, while salt rejection

433   was also enhanced with increasing numbers of SWCNT printings. Improvement of water flux

434   at higher printing numbers (between 0 to 10 cycles) could mainly be attributed to the formation

435   of significantly thinner PA layer (see Fig. 5, reduced from 123.5 ± 9.4 nm to 56.9 ± 6.8 nm).

436   Thus, the thinner PA active layer subsequently reduced the water transport resistance and the

437   porous SWCNT interlayer matrix provide increase in liquid transport channels, and such trend

438   is in good agreement with other literatures [12, 15, 32]. Additionally, a higher degree of

439   cross-linking of PA layers (Table 2) formed on the PES substrates containing SWCNT

440   interlayers (i.e. TP-5 and TP-10), as compared to TP-0 (without SWCNT interlayer), could

441   enhance the ion selectivity with minimized water permeance hindrance.

442
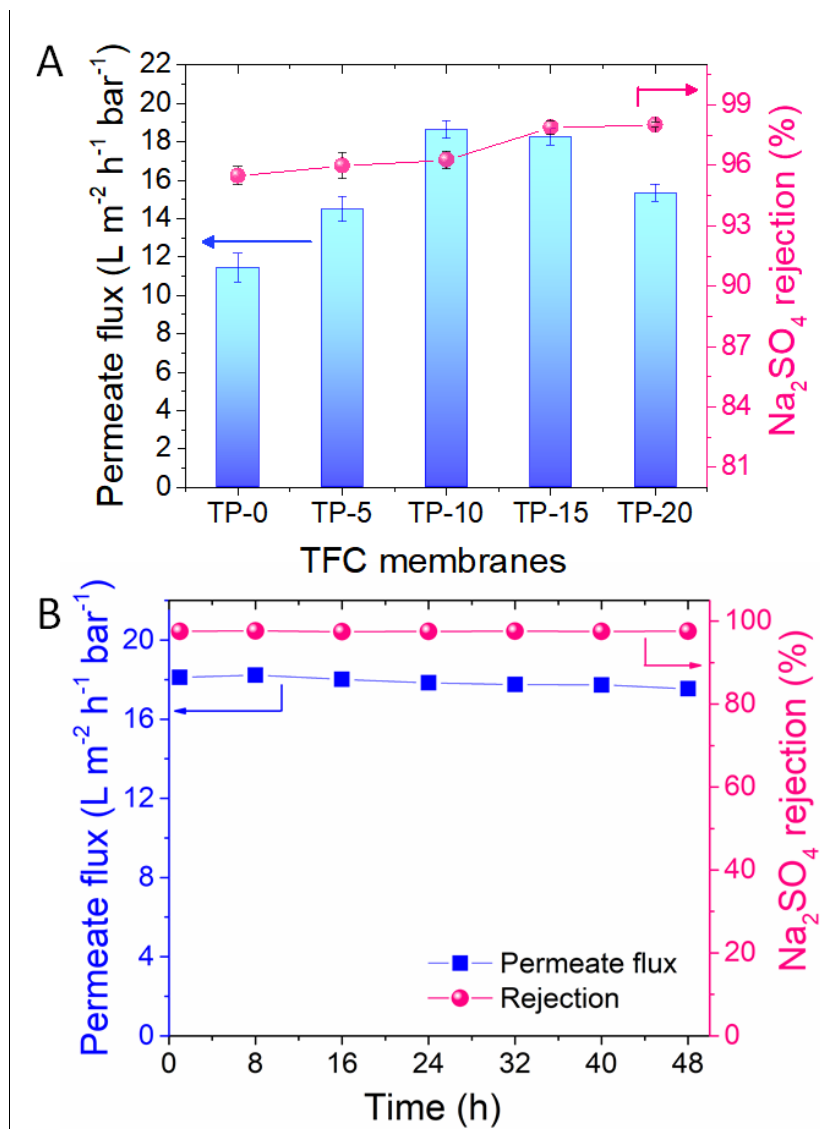
Fig. 7. (A) Permeate water flux and salt rejection performances of the TFC NF membranes fabricated with different numbers of SWCNT prints and (B) long-term performance of the TP-15 membrane (feed solution: Na_2SO_4 1,000 mg L^{-1}, applied pressure: 4 bar, and cross-flow velocity: 0.83 cm s^{-1}).

447

448   Meanwhile, TP-20 membrane, exhibited the water flux of 15.31 ± 0.43 L m^{-2} h^{-1} bar^{-1} revealing

449   slight reduction in flux when compared with TP-10 or TP-15 membranes, yet higher than that

450   of TP-0 membrane. Moreover, TP-20 membrane exhibited further enhanced salt rejection of

451 Na$_2$SO$_4$ up to 98.01 ± 0.14%. Further deposition of SWCNT interlayer on PES MF support

452 (e.g. 20 cycles of SWCNT prints) resulted in formation of thinnest PA active layer (41.7 nm)

453 among all TFC membranes (Fig. 5). However, this also led to the highest degree of PA layer

454 crosslinking (Table 2) which resulted in tightening of the membrane pore size attributing to the

455 slightly reduced water permeance [14]. Amongst all prepared TFC membranes with varying

456 number of SWCNT printing cycles, P-15 support membrane (15 cycle SWCNT prints)

457 provided the best support membrane condition for IP process which resulted in both high water

458 flux (18.24 ± 0.43 L m^{-2} h^{-1} bar^{-1}) and excellent salt rejection rate compared to other membranes.

459 Further experiment using the TP-15 membrane was also conducted to investigate the

460 membrane stability under long-term operation. As shown in Fig. 7(B), both water permeability

461 and salt rejection performances remained constant during the operation for 48 hours,

462 confirming the good mechanical stability of the fabricated TFC membrane.

463
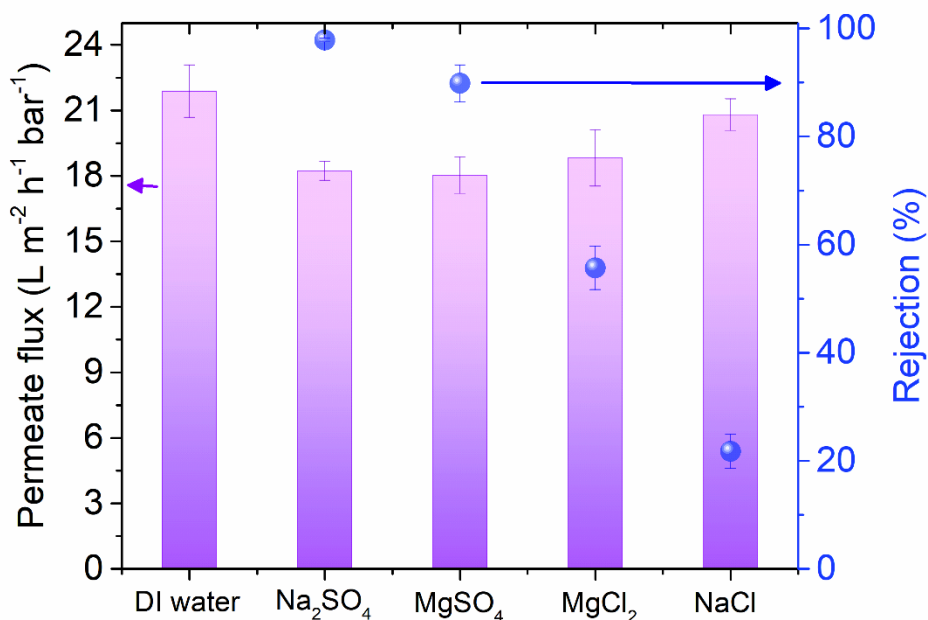
464

465   **Fig. 8**. Permeate water flux and rejection performances of TP-15 TFC NF membrane (15

466   SWCNT prints) under varied salts as a feed solution (1,000 mg L^{-1} Na$_2$SO$_4$, MgSO$_4$, MgCl$_2$

467   and NaCl) and DI water, applied pressure: 4 bar.

468   The NF separation performance for the TP-15 TFC membrane was further evaluated with

469   different salts as well as DI water as feed waters and their permeate flux and salts rejection

470   results can be seen in Fig. 8. It can be note that the rejection rate of salts by TP-15 TFC

471   membrane showed in the order of Na$_2$SO$_4$ (97.88 ± 0.33%), MgSO$_4$ (89.78 ± 3.42%), MgCl$_2$

472   (55.71 ± 4.02%) and NaCl (21.76 ± 3.13%). The sulfate salts such as Na$_2$SO$_4$ and MgSO$_4$

473   exhibited much higher rejection rates than that of chloride salts including MgCl$_2$ and NaCl

474   because the synergistic effect of molecular size sieving and strong Donnan exclusion (IEP ≈5.6

475   for TP-15) with the sulfate salts [10, 15, 31]. The TP-15 TFC membrane achieved the pure

476   water flux (DI water as feed) of 21.89 ± 1.20 L m^{-2} h^{-1} bar^{-1} and when saline solution was used

477   as feed, lower permeate fluxes were observed for all cases of feed solution containing varying

478   salts due to the hindrance by osmotic pressure of each salts and concentration polarization.

479
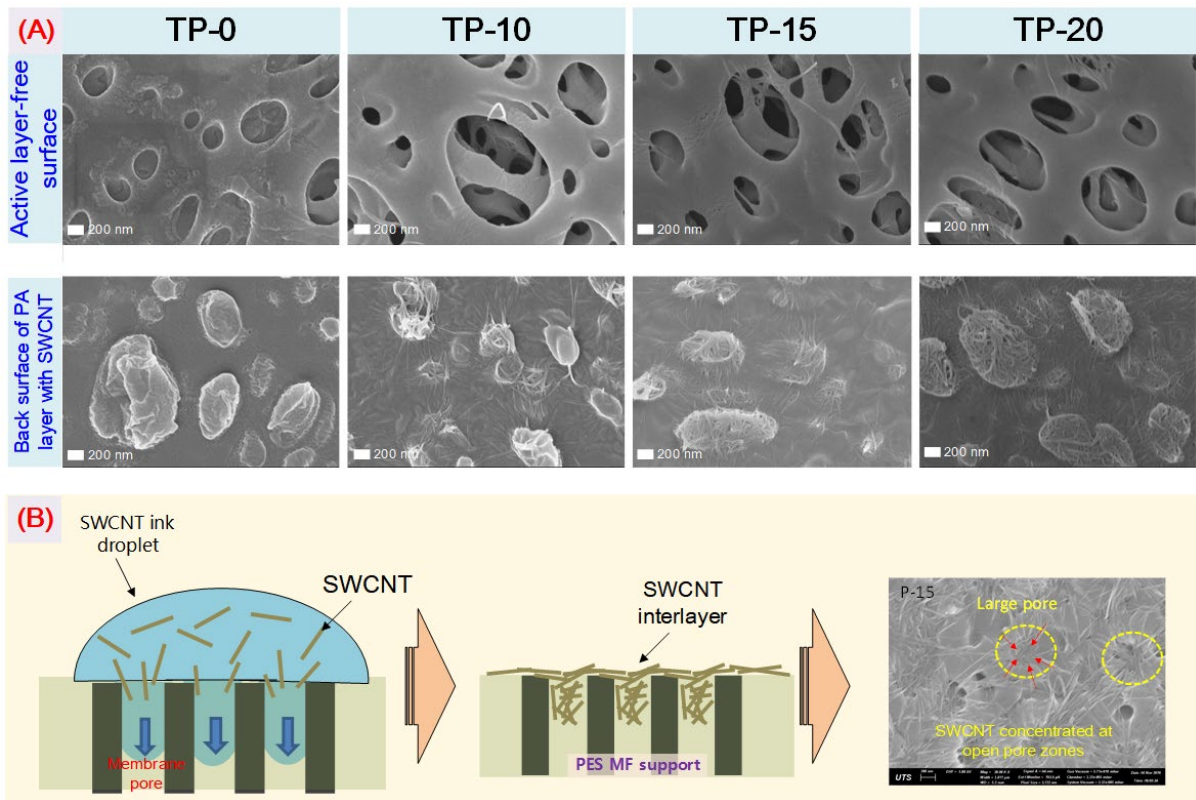
Fig. 9. Morphology changes of PA selective layers formed on varying number of SWCNT printings characterized by FE-SEM (A) for active layer (PA or PA with SWCNT)-free surface and back surface of PA layer with SWCNT interlayer, and (B) conceptual illustration of SWCNT ink drop on PES MF support depositing the SWCNT interlayer.

3.5 Implication and limitation of SWCNT interlayers utilized via inkjet printing

To further explore the formation of PA active layers as well as their morphology changes on different loadings of SWCNT coated via inkjet printing process, active layer (PA alone or PA with SWCNT) on the TFC membranes were carefully removed using an adhesive tape. Then the morphologies of active layer-free surfaces of PES membrane (active layer removed) and the back surfaces of PA without SWCNT (TP-0) and PA with SWCNT (TP-10, TP-15 and TP-20) layers were investigated by FE-SEM observation as shown in Fig. 9(A). Numbers of

27

493   nodular-shaped, non-porous particles appeared on the back surface of PA layer for TP-0

494   membrane. This is due to the presence of large pores of PES surface, leading to uneven

495   coverage by PIP aqueous solution allowing the facile penetration of TMC solvent into the

496   larger pore structures during the IP process, causing the formation of PA particles inside the

497   micropores of PES support [12, 32]. While, active layer-free surface image of TP-0 membrane

498   revealed some remainder of the dense PA active layers formed inside the pores which were not

499   fully detached from the surface of PES support by an adhesive tape. This indicates that the

500   discontinuous PA layer was formed on the pure PES support. However, other samples which

501   had SWCNT interlayer such as TP-10, -15 and -20 membranes, where active layers were

502   composed of PA and SWCNT, revealed the typical surface structure of PES MF membrane

503   when active layer was completely peeled-off. Interestingly, nodular shaped particles were also

504   observed on the back surface from the membrane samples (TP-10~20) shown in FE-SEM

505   images, where those particles were mainly composed of porous SWCNTs bundles. This trend

506   clearly shows that, with increase of SWCNT printing numbers, the dense PA nodular particles,

507   on the back surface of PA layer were non-visible when SWCNT prints exceeded 10 cycles (TP-

508   15 and TP-20). This observation reinforces our claim that PES support membrane pores were

509   fully covered and occupied with SWCNT matrix on the PES membrane surface, reducing the

510   surface pore size and smoother surface with interconnected matrix, providing a buffer layer

511   which facilitates the uniform distribution of PIP monomer in the membrane substrate, leading

512   to formation of smoother and low-defect PA layer. Also substrate surface tuned by SWCNT

513   deposition limits the diffusion of the PIP monomer during the IP process, leading to formation

514   of thinner PA layer with higher degree of cross-linking (Table 1) [12].

515   We also noticed that the back surface structures of support membrane coated with SWCNT

516   via inkjet printing serve as an interlayer, after the IP process. This new information reveals that

517   the SWCNTs interlayer structure exhibits a flat-nodular shaped patterns which are slightly

518 different to other literatures which report flat surface on the back side of PA layer with low

519 roughness and imprinted patterns of SWCNT matrix [12, 32]. In previous studies, CNTs were

520 mostly coated on a MF support via vacuum filtration method [8, 10-12, 15], or other few studies

521 used spray coating [32] or brush-painting [31] techniques. These nanomaterial coating

522 techniques are mainly pressurized or force-driven techniques where most of the CNTs will be

523 positioned and composed as interconnected matrix on the membrane surface covering the

524 surface pores. However, as illustrated in Fig. 9(B), SWCNTs deposition via inkjet printing is

525 sensitive to the surface morphology of microporous support membrane. When a pico-liter of

526 SWCNTs ink droplet comes in contact with a surface of PES support, ink would first move to

527 larger and inner pores which have lower capillary force and mass transport resistance. A high

528 surface tension of SWCNT water based ink ($\approx$ 72 dynes cm^{-1}) might also affect the water

529 penetration behaviors. Thus, the SWCNTs will accumulate partially in the area of inner pores

530 and when the pores sufficiently filled, then SWCNTs layer will fully cover the other regions

531 on the PES membrane surface. This orderly deposited SWCNTs via inkjet printing resulted in

532 slightly different patterns of the back surface of PA-SWCNT layers (see Fig. 9(A, B)). Such

533 unique formation of PA-SWCNT selective layer would possibly aid in binding between the PA

534 selective layer and PES support layer, forming a mechanically stable SWCNT intermediate

535 layer between PES support and PA layer, as long-term experiment confirms the stability of

536 TFC membranes (see Fig. 7(b)). Moreover, SWCNT with short lengths of 1~3 μm was used as

537 SWCNT ink in this study (in previous studies, SWCNT with size of 5~30 μm were used), and

538 this could be another reason for the ease in penetration of the SWCNTs into the pores of PES

539 support. We also attempted to use the SWCNTs sizes of 5~30 μm as an ink, however, easy

540 blockage of ink nozzle head was observed even at low SWCNT concentration, as nozzle

541 diameter was only 30 μm. As we used a commercial HP home-office inkjet printer and inkjet

542 cartridge, the nozzle size of cartridge could not be adjusted and caused the limitation in

543 designing and demonstration while changing other printing parameters. Nevertheless, we

544 demonstrate the high potential of using inkjet printing technology to coat nanomaterials for

545 membrane developments and further investigations are needed to develop suitable

546 nanomaterial inks and printing devices optimization in near future.

547 *3.6 Conclusions*

548   A high performance TFC NF membrane with ultrathin PA active layer was successfully

549 synthesized by using SWCNTs as an interlayer between the PA active layer and PES MF

550 membrane support. We first introduced a potential application of inkjet printing technology to

551 deposit SWCNT ink on PES MF membrane to utilize them as an interlayer. SWCNT ink printed

552 over 10 cycles efficiently modified the surface morphology of PES MF support membrane by

553 reducing surface pore size and roughness, thereby achieving a formation of ultrathin PA active

554 layer (PA layer thickness of TP-15 is ~42 nm). The TFC NF membrane fabricated at an optimal

555 condition (15 cycle prints of SWCNT ink) exhibited significantly improved membrane

556 performances including permeate water flux of 18.24 ± 0.43 L m^{-2} h^{-1} bar^{-1} with a high salt

557 rejection of Na$_2$SO$_4$ divalent salts ($97.88 \pm 0.33\%$) as compared to SWCNT-free TFC

558 membrane. We also demonstrate that inkjet printing technique is an attractive route for

559 depositing nanomaterials, which is simple and enable rapid deposition with potential scalability

560 on the membranes surface not only for SWCNT ink, but which could also be applicable for

561 depositing other nanomaterials. However, some challenges of inkjet printing technology yet

562 remains to be overcome in future, such as further efforts in developing optimum nanomaterial

563 inks and development of printing devices specialized for membrane manufacturing.

564

References

[1] X. Hao, S. Gao, J. Tian, Y. Sun, F. Cui, C.Y. Tang, Calcium-Carboxyl Intrabridging during Interfacial Polymerization: A Novel Strategy to Improve Antifouling Performance of Thin Film Composite Membranes, Environ Sci Technol, 53 (2019) 4371-4379.

[2] K.P. Lee, J. Zheng, G. Bargeman, A.J.B. Kemperman, N.E. Benes, pH stable thin film composite polyamine nanofiltration membranes by interfacial polymerisation, Journal of Membrane Science, 478 (2015) 75-84.

[3] W. Choi, S. Jeon, S.J. Kwon, H. Park, Y.-I. Park, S.-E. Nam, P.S. Lee, J.S. Lee, J. Choi, S.J.J.o.M.S. Hong, Thin film composite reverse osmosis membranes prepared via layered interfacial polymerization, 527 (2017) 121-128.

[4] A.F. Ismail, M. Padaki, N. Hilal, T. Matsuura, W.J. Lau, Thin film composite membrane — Recent development and future potential, Desalination, 356 (2015) 140-148.

[5] A.W. Mohammad, Y.H. Teow, W.L. Ang, Y.T. Chung, D.L. Oatley-Radcliffe, N. Hilal, Nanofiltration membranes review: Recent advances and future prospects, Desalination, 356 (2015) 226-254.

[6] S. Karan, Z. Jiang, A.G. Livingston, Sub-10 nm polyamide nanofilms with ultrafast solvent transport for molecular separation, Science, 348 (2015).

[7] Y. Liang, C. Li, S. Li, B. Su, M.Z. Hu, X. Gao, C. Gao, Graphene quantum dots (GQDs)-polyethyleneimine as interlayer for the fabrication of high performance organic solvent nanofiltration (OSN) membranes, Chemical Engineering Journal, 380 (2020).

[8] M.-B. Wu, Y. Lv, H.-C. Yang, L.-F. Liu, X. Zhang, Z.-K. Xu, Thin film composite membranes combining carbon nanotube intermediate layer and microfiltration support for high nanofiltration performances, Journal of Membrane Science, 515 (2016) 238-244.

[9] P. Gorgojo, S. Karan, H.C. Wong, M.F. Jimenez-Solomon, J.T. Cabral, A.G. Livingston, Ultrathin Polymer Films with Intrinsic Microporosity: Anomalous Solvent Permeation and High Flux Membranes, Advanced Functional Materials, 24 (2014) 4729-4737.

[10] Y. Zhu, W. Xie, S. Gao, F. Zhang, W. Zhang, Z. Liu, J. Jin, Single-Walled Carbon Nanotube Film Supported Nanofiltration Membrane with a Nearly 10 nm Thick Polyamide Selective Layer for High-Flux and High-Rejection Desalination, Small, 12 (2016) 5034-5041.

[11] K. Goh, L. Setiawan, L. Wei, W. Jiang, R. Wang, Y. Chen, Fabrication of novel functionalized multi-walled carbon nanotube immobilized hollow fiber membranes for enhanced performance in forward osmosis process, Journal of Membrane Science, 446 (2013) 244-254.

[12] G. Gong, P. Wang, Z. Zhou, Y. Hu, New Insights into the Role of an Interlayer for the Fabrication of Highly Selective and Permeable Thin-Film Composite Nanofiltration Membrane, ACS applied materials & interfaces, 11 (2019) 7349-7356.

[13] M. Wu, J. Yuan, H. Wu, Y. Su, H. Yang, X. You, R. Zhang, X. He, N.A. Khan, R. Kasher, Z. Jiang, Ultrathin nanofiltration membrane with polydopamine-covalent organic framework interlayer for enhanced permeability and structural stability, Journal of Membrane Science, 576 (2019) 131-141.

[14] J.-J. Wang, H.-C. Yang, M.-B. Wu, X. Zhang, Z.-K. Xu, Nanofiltration membranes with cellulose nanocrystals as an interlayer for unprecedented performance, Journal of Materials Chemistry A, 5 (2017) 16289-16295.

[15] Z. Wang, Z. Wang, S. Lin, H. Jin, S. Gao, Y. Zhu, J. Jin, Nanoparticle-templated nanofiltration membranes for ultrahigh performance desalination, Nature Communications, 9 (2018) 2004.

[16] W. Choi, S. Jeon, S.J. Kwon, H. Park, Y.-I. Park, S.-E. Nam, P.S. Lee, J.S. Lee, J. Choi, S. Hong, E.P. Chan, J.-H. Lee, Thin film composite reverse osmosis membranes prepared via layered interfacial polymerization, Journal of Membrane Science, 527 (2017) 121-128.

[17] X. Zhang, Y. Lv, H.C. Yang, Y. Du, Z.K. Xu, Polyphenol Coating as an Interlayer for Thin-Film Composite Membranes with Enhanced Nanofiltration Performance, ACS applied materials & interfaces, 8 (2016) 32512-32519.

[18] M. Singh, H.M. Haverinen, P. Dhagat, G.E. Jabbour, Inkjet printing-process and its applications, Advanced materials, 22 (2010) 673-685.

[19] J.L. Zhuang, D. Ar, X.J. Yu, J.X. Liu, A. Terfort, Patterned deposition of metal-organic frameworks onto plastic, paper, and textile substrates by inkjet printing of a precursor solution, Advanced materials, 25 (2013) 4631-4635.

[20] C.J. Zhang, L. McKeon, M.P. Kremer, S.H. Park, O. Ronan, A. Seral-Ascaso, S. Barwich, C.O. Coileain, N. McEvoy, H.C. Nerl, B. Anasori, J.N. Coleman, Y. Gogotsi, V. Nicolosi, Additive-free MXene inks and direct printing of micro-supercapacitors, Nat Commun, 10 (2019) 1795.

[21] N. Karim, S. Afroj, A. Malandraki, S. Butterworth, C. Beach, M. Rigout, K.S. Novoselov, A.J. Casson, S.G. Yeates, All inkjet-printed graphene-based conductive patterns for wearable e-textile applications, Journal of Materials Chemistry C, 5 (2017) 11640-11648.

[22] M. Zeng, Y. Zhang, Colloidal nanoparticle inks for printing functional devices: emerging trends and future prospects, Journal of Materials Chemistry A, 7 (2019) 23301-23336.

[23] B.J. de Gans, P.C. Duineveld, U.S. Schubert, Inkjet Printing of Polymers: State of the Art and Future Developments, Advanced materials, 16 (2004) 203-213.

[24] J. Li, F. Rossignol, J. Macdonald, Inkjet printing for biosensor fabrication: combining chemistry and technology for advanced manufacturing, Lab Chip, 15 (2015) 2538-2558.

[25] S. Kholghi Eshkalak, A. Chinnappan, W.A.D.M. Jayathilaka, M. Khatibzadeh, E. Kowsari, S. Ramakrishna, A review on inkjet printing of CNT composites for smart applications, Applied Materials Today, 9 (2017) 372-386.

[26] E.B. Secor, P.L. Prabhumirashi, K. Puntambekar, M.L. Geier, M.C. Hersam, Inkjet Printing of High Conductivity, Flexible Graphene Patterns, J Phys Chem Lett, 4 (2013) 1347-1351.

[27] C. Wang, M.J. Park, D.H. Seo, H.K. Shon, Inkjet printing of graphene oxide and dopamine on nanofiltration membranes for improved anti-fouling properties and chlorine resistance, Separation and Purification Technology, 254 (2021).

[28] M. Fathizadeh, H.N. Tien, K. Khivantsev, J.-T. Chen, M. Yu, Printing ultrathin graphene oxide nanofiltration membranes for water purification, J. Mater. Chem. A, 5 (2017) 20860-20866.

[29] M.J. Park, S. Phuntsho, T. He, G.M. Nisola, L.D. Tijing, X.-M. Li, G. Chen, W.-J. Chung, H.K. Shon, Graphene oxide incorporated polysulfone substrate for the fabrication of flat-sheet thin-film composite forward osmosis membranes, Journal of Membrane Science, 493 (2015) 496-507.

[30] M.J. Park, R.R. Gonzales, A. Abdel-Wahab, S. Phuntsho, H.K. Shon, Hydrophilic polyvinyl alcohol coating on hydrophobic electrospun nanofiber membrane for high performance thin film composite forward osmosis membrane, Desalination, 426 (2018) 50-59.

[31] S. Gao, Y. Zhu, Y. Gong, Z. Wang, W. Fang, J. Jin, Ultrathin Polyamide Nanofiltration Membrane Fabricated on Brush-Painted Single-Walled Carbon Nanotube Network Support for Ion Sieving, ACS Nano, 13 (2019) 5278-5290.

661 [32] Z. Zhou, Y. Hu, C. Boo, Z. Liu, J. Li, L. Deng, X. An, High-Performance Thin-Film
662 Composite Membrane with an Ultrathin Spray-Coated Carbon Nanotube Interlayer,
663 Environmental Science & Technology Letters, 5 (2018) 243-248.

664